Non-line-of-sight imaging

Daniele Faccio, Andreas Velten and Gordon Wetzstein

Abstract | Emerging single-photon-sensitive sensors produce picosecond-accurate time-stamped photon counts. Applying advanced inverse methods to process these data has resulted in unprecedented imaging capabilities, such as non-line-of-sight (NLOS) imaging. Rather than imaging photons that travel along direct paths from a source to an object and back to the detector, NLOS methods analyse photons that travel along indirect light paths, scattered from multiple surfaces, to estimate 3D images of scenes outside the direct line of sight of a camera, hidden by a wall or other obstacles. We review the transient imaging techniques that underlie many NLOS imaging approaches, discuss methods for reconstructing hidden scenes from time-resolved measurements, describe some other methods for NLOS imaging that do not require transient imaging and discuss the future of 'seeing around corners'.

The ability to image objects outside the direct line of sight of a camera would enable applications in robotic vision, remote sensing, medical imaging, autonomous driving and many other domains. For example, the ability to see hidden obstacles could enable autonomous vehicles to avoid collisions, drive more efficiently and plan driving actions further in advance. Present-day 3D imaging systems commonly used in automotive sensing, such as light detection and ranging (LiDAR), measure the time it takes a light pulse to travel along a direct path from a source to a visible object and back to a sensor. Non-line-of-sight (NLOS) imaging goes one step further by analysing light scattered from multiple surfaces along indirect paths, with the goal of revealing the 3D shape and visual appearance of objects outside the direct line of sight[1,2] (FIG. 1).

NLOS imaging poses several challenges. One challenge is that only a few of the many recorded photons carry the information necessary to estimate hidden objects. Whereas the photon count of light directly reflected from a single scattering point falls off with a factor proportional to the inverse of the square distance, the signal strength of light scattered from multiple surfaces decreases several orders of magnitude faster. Robustly detecting and time-stamping the few indirectly scattered photons in the presence of the much brighter signal returning directly from the visible scene requires single-photon-sensitive detectors with a high dynamic range or with gating capabilities. A second challenge is that the inverse problem of estimating 3D shape and appearance of hidden objects from intensity measurements alone is ill-posed. Solving the NLOS problem robustly requires advanced imaging systems capable of picosecond-accurate time-resolved measurement, mathematical priors on the imaged scenes, or other unconventional approaches. A third challenge is that the inverse problems associated with NLOS imaging are extremely large. Developing efficient algorithms to compute solutions in reasonable times and with memory resources available on a single computer is crucial to make this emerging imaging modality practical.

Over the past 8 years, various approaches addressing the NLOS problem have been proposed. Some of these focus on advanced measurement systems, using femtosecond and picosecond time-resolved detectors[2–5], interferometry[6,7], acoustic systems[8], passive imaging systems[9–11] or thermal imaging[12,13]. Others explore models of light transport that make certain assumptions on the reflectance or other properties of the hidden scenes. At the convergence of physics, signal processing, optics and electronics, NLOS imaging is an interdisciplinary challenge that has seen much progress. Nevertheless, continued effort in both theory and experimental systems is necessary to make the idea of seeing around corners practical 'in the wild'.

Time-resolved imaging systems that use pulsed light sources along with single-photon detectors are some of the most promising candidates for practical solutions in NLOS imaging. The measurement process of time-resolved NLOS imaging systems can be understood from an example scene in which a pulsed laser with a pulse width in, for example, the range 100 fs to 100 ps, illuminates a wall that acts as a relay surface at one point (FIG. 1a). The light reaching the wall subsequently scatters into the hidden region where it re-scatters off any hidden objects before returning to the wall where the time-resolved indirect light transport is measured. Individual areas on the object scatter back spherical waves, which upon intersecting the wall give rise to ellipsoids that expand outwards in time (shown schematically in FIG. 1b). It is these time-varying ellipsoids that contain all the information required to reconstruct a full 3D image of the hidden scene. The key requirement for time-resolved NLOS approaches is the temporal resolution of the detector, which must be high enough to freeze light in motion[14] (FIG. 1c). Light travels ~3 cm in 100 ps, which determines the desired temporal resolution of the imaging system, because this dictates the achievable transverse and axial resolution of reconstructed 3D images.

In this Perspective, we discuss the emerging field of NLOS imaging and aim at making it accessible to the reader by categorizing existing approaches by the types of measurement systems they use and their algorithmic approaches. We first discuss technologies that enable imaging at the speed of light: that is, detectors with femtosecond or picosecond accuracy. We then discuss time-resolved NLOS imaging approaches that build on these technologies. Finally, we overview alternative methods for NLOS imaging and discuss possible future directions of the field.

Imaging at the speed of light

The concept of freezing light in motion, sometimes referred to as 'light-in-flight' or 'transient' imaging, is not specific to

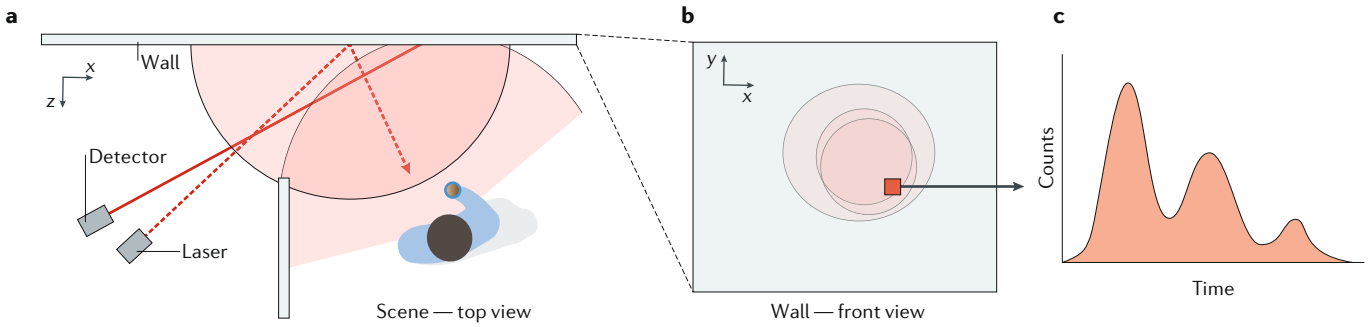

Fig. 1 | **Layout of time-resolved non-line-of-sight imaging. a** | A visible wall is illuminated with a pulsed laser source. Light scattered from this wall extends into the obscured region and indirectly illuminates hidden objects, which in turn scatter the light back to the wall where it is recorded by a time-resolved detector, typically a single-photon avalanche diode (SPAD) sensor. **b** | Schematic of the waves scattered from the hidden object on the observation wall when 'frozen' at a given time. The ellipsoids observed on the wall are the intersection with the wall of spherical scattered waves from the object. **c** | Schematic of the temporal trace of photon counts observed at a given pixel on the wall. The peaks correspond to the scattered spherical waves expanding outwards with time.

NLOS imaging[14]. Several techniques for light-in-flight imaging have been proposed, starting in the 1960s when nonlinear optical gating techniques were first used to create an ultrafast shutter. Doing so extended the basic concept of the mechanical shutter used in many high-speed cameras to that of a shutter that is activated by light itself. Another ingenious approach that effectively paved the way for true light-in-flight imaging was developed in the 1970s and relies on standard holographic techniques[15], modified so that the reference field is a laser pulse that is spatially extended and hits the photographic plate at an angle[16–19]. The result is a hologram in which different transverse locations on the exposed photographic plate correspond to different times in the scene, owing to the different arrival times of the tilted reference pulse. Viewing the photographic plate at different lateral positions provides an image at different times with resolutions of the order of picoseconds or even less. A related technique that also relies on interference of the light reflected from a scene or object with a reference field is based on a generalization of optical coherence tomography. Reconstructions of transient light scenes with very high spatial resolution (tens of micrometres) with 15 trillion frames per second are obtained through detection of interference fringes as the interferometer delay is varied[20]. Despite the success of these and related approaches, their application has been limited to scenes that are relatively simple.

Transient imaging using time-of-flight cameras provides a 3D image of a scene that can also be applied to NLOS[21–23] and offers the distinct advantage of being low budget, with commercial time-of-flight cameras costing around US$100. These cameras illuminate the scene with a sinusoidally modulated (typically 10–100 MHz or higher) light beam. The return signal is demodulated against a reference sine wave from which a phase delay is extracted that is directly related to the time of flight and hence to the propagation distance within the scene (see REFS[14,24] for an overview).

Higher temporal resolution and better light sensitivity, both key parameters for NLOS imaging, can be obtained with more complex and expensive cameras. For example, full 3D NLOS imaging was first demonstrated with a streak camera, which enabled precise reconstruction of a small mannequin[2] (FIG. 2). These cameras rely on a photocathode to convert the incoming photons into electrons. The electrons can then be 'streaked' by a time-varying electric field, thereby mapping time onto transverse position. The streaked electrons are detected on a standard charge-coupled device (CCD) camera after reconversion back into photons on a phosphor screen. The use of one spatial dimension for the temporal streaking implies that these cameras can only see one line of the scene at a time, a limitation that can be offset for NLOS imaging by scanning the illumination laser spot[2,25]. Techniques have been implemented that make it possible to fully open the input slit and, by computational fusion with data from a CCD, obtain a full 2D image without any need for scanning[26–28]. Interestingly, these full-imaging approaches have not yet been applied to NLOS imaging.

An alternative approach to transient imaging is based on the use of intensified CCD cameras (iCCD). iCCDs rely on a microchannel plate that is electronically gated so that electrons generated by an input photocathode are amplified only for a short gate time before being reconverted back to light on a phosphor screen and detected on a CCD or complementary metal–oxide–semiconductor (CMOS) camera. Typical gate times are of the order of nanoseconds but can be as short as 100 ps, or even less. Like all of the imaging techniques reviewed here, iCCDs can also be used for NLOS imaging[29].

These and later techniques applied to light-in-flight imaging have sufficient precision to observe distortions in the final video due to the finite speed of light, such as apparently inverted motion of refracted waves from a bottle or apparent superluminal motion of light pulses[30,31]. A 100-ps-gate iCCD has been used to record the apparent time reversal of events occurring during light propagation: the intersection of a plane wave and a wall travels at speed $c/\sin\theta$ (θ is the intersection angle between the plane wave and the wall) and is therefore always superluminal. The transient imaging of the scattering of light from this intersection plane on the wall reveals an apparent motion in the direction opposite to that actually followed by the light pulse[32], in much the same way that a piece of music played by a speaker moving faster than the speed of sound is heard backwards[33].

Moving beyond the first 3D NLOS imaging based on streak cameras[2], work ensued to improve on some of the limitations encountered in these measurements that required several hours of data acquisition. There was particular emphasis on improving acquisition speed (with the goal of video frame-rate imaging), light sensitivity (aiming to extend the observation area to entire rooms and observe human-sized objects), portability (for deploying the technology in the real world) and cost (ideally, there would be a technology that does all the above with similar costs to a time-of-flight camera).

Single-photon avalanche diodes (SPADs) are semiconductor structures similar to a photodiode but with a large bias voltage, which results in carrier multiplication: the absorption of a single photon causes an avalanche breakdown, leading to a large current signal that can be detected and processed by external electronics. Time-to-digital converters measure the time between the emission of an illumination pulse and the detection of an associated returned photon on the SPAD. A time-correlated single-photon counter is then used to form a histogram of photon arrival times[34]. SPADs achieve single-photon sensitivity with photon detection efficiencies up to 40% and exceptionally low dark count rates of 1–10 photons per second in the visible spectrum. After the detection of a photon, the detector is blind for a hold-off period (dead time) of tens to hundreds of nanoseconds, thus limiting the achievable maximum count rate. The histogram of photon arrival times gives a precise measurement of the light pulse temporal profile, as long as the measurement is performed in a photon-sparse regime — that is, a regime in which the likelihood of more than one photon hitting the detector during the dead time (referred to as pile-up) is substantially less than one. Accounting for the SPAD dead time, working in the photon-sparse regime provides a maximum allowed count rate, avoiding photon pile-up distortion effects, of the order of 1–10 MHz.

SPAD detectors are available in both single-pixel and arrayed (that is, camera) format, at both visible[35–46] and infrared wavelengths[47–49]. SPAD cameras have been used for light-in-flight imaging, for which the single-photon sensitivity enabled the camera to capture a light pulse propagating in free space, with photons collected on the camera originating from Rayleigh scattering in air, as opposed to scattering from a surface or enhanced scattering in a diffusive medium[50] (FIG. 3). The 32 × 32 pixel SPAD camera had a temporal resolution of about 50 ps, corresponding to 200 million frames per second. Although not as fast as some of the techniques discussed above that can attain more than a trillion frames per second, this frame rate is still sufficient to freeze light in motion with a blur of only 1.5 cm. This minor loss of temporal resolution comes with several benefits. The cameras are compact, are straightforward to use (the camera is based on standard CMOS technology, is commercially available and is small enough to be integrated into a smartphone), have high data acquisition rates (NLOS data acquisition has been demonstrated with sub-second timescales)[51] and, with interference filters at the specific laser illumination wavelength, can also be deployed outdoors and in daylight conditions[3,52]. Video frame-rate acquisition of transient images using SPADs has been achieved[53], as well as in more standard LiDAR configurations deployed outdoors over kilometre distances[54].

The first application of SPAD array sensors to NLOS imaging was in a simpler configuration in which only the position of the target was assessed, rather than its full 3D shape. This simplification allowed acquisition and processing times of the order of 1 second for a moving target, both in a small-scale laboratory set-up[55] and also for detecting people behind a corner on larger scales (more than 50 m distance from the detector)[52]. Single-pixel gated SPADs[56] and line arrays[57] with a scanning laser spot have also been used to acquire full 3D scenes and are currently some of the preferred approaches for NLOS imaging, with most set-ups over the past few years using SPADs either in single pixel or array format.

The temporal resolution actually required from the detector depends on factors that include the illumination pulse length and the task at hand. For example, for transient imaging, such as capturing a light pulse in flight, there is no need to use a detector with temporal resolution shorter than the pulse length. For 100-ps or longer pulses, this can readily be achieved with the techniques described above. For femtosecond pulses, such as those available from standard femtosecond oscillators, the current resolution of detectors, limited to 10 or more picoseconds, will unavoidably result in temporal blur of the pulse that will be of order 0.3–1 cm, compared with the 30 μm of a 100-fs pulse. However, when considering NLOS imaging, the detector's temporal resolution directly affects both transverse and depth resolution of the 3D image reconstruction, as discussed below.

At present, most SPAD arrays are developed for LiDAR imaging. Looking to the future, NLOS applications require improvements in temporal resolutions, better fill factors, the ability to gate out direct light from the relay surface, and a more flexible way to read out photon time stamps from those SPAD pixels that see a photon. There is therefore a need for SPAD arrays specifically designed with NLOS applications in mind.

Time-of-flight NLOS imaging

Image formation model

A time-resolved detector, such as a SPAD, measures the incident photon flux as a function of time, relative to an emitted light pulse. The detector is therefore used to record the temporal impulse response of a scene, including direct and global illumination, at sampling positions x', y' on a visible surface (FIG. 1), resulting in a 3D space–time volume that is referred to as the transient image, τ. As discussed in the previous section, a transient image contains both directly reflected photons and photons that travel along indirect light paths. The direct illumination (that is, light emitted by the source and scattered back to the detector from an object) contains all information necessary to recover the shape and reflectance of visible parts of the scene. Recovering such information is commonly done for 3D imaging and LiDAR. For NLOS imaging, the direct light is typically not considered because it does not contain useful information on the hidden scene. It can be readily removed from measurements, for example by using the fact that it arrives earlier than multiple-surface reflected photons, and can therefore be gated out.

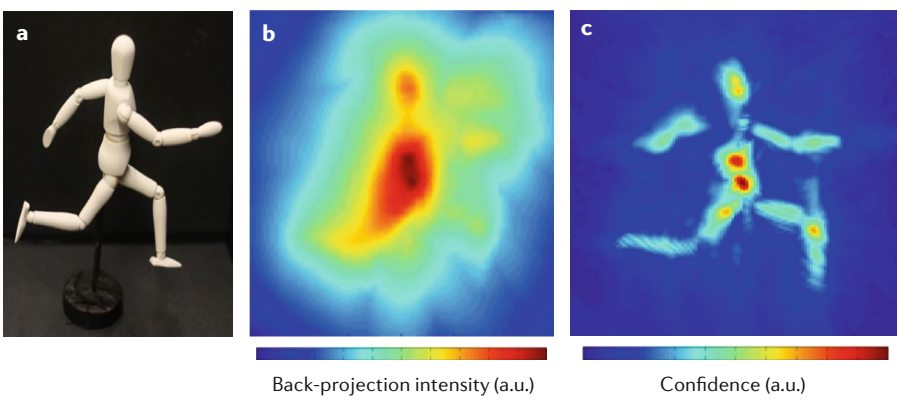

Fig. 2 | **First experimental demonstration of 'looking around corners'.** A mannequin behind a corner (panel **a**) is recovered from time-resolved measurements using unfiltered (panel **b**) and filtered (panel **c**) back-projection algorithms. Adapted from REF.[2], Springer Nature Limited.

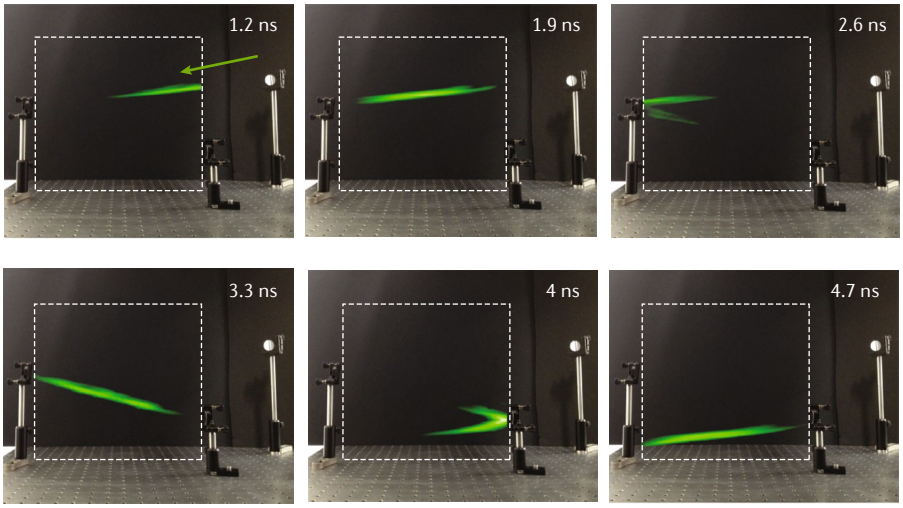

Fig. 3 | **Demonstration of the capability of recording light in flight at picosecond timescales for a pulse of light propagating between three mirrors.** Such time-resolved measurements of light transport form the basis of many non-line-of-sight imaging techniques. The laser light first hits the small circular mirror on the right and is directed towards the field of view of the single-photon avalanche diode (SPAD) camera, as indicated by the arrow in the first image. The field of view (FOV) is represented by dashed rectangles and corresponds to a region $35 \times 35\ \mathrm{cm}^2$. In the successive frames the laser pulse is imaged at increasing times, indicated in each frame, before exiting the FOV in the last frame. Adapted from REF.[50], CC BY 4.0.

The image formation model for the time-resolved indirect light transport of a confocal NLOS system[3] (that is, one in which both the laser illumination and the subsequent detection are at the same point x',y' on the visible surface) can be formulated as

$$\tau(x',y',t) = \iiint_{\Omega} \frac{1}{r^4}\rho(x,y,z)\, g(x',y',x,y,z)\, \delta\left(2\sqrt{(x'-x)^2+(y'-y)^2+z^2}-tc\right) \mathrm{d}x\mathrm{d}y\mathrm{d}z, \quad (1)$$

where ρ is the reflectance of a point in the hidden scene and the Dirac delta function δ relates the time of flight t to the distance function $r=\sqrt{(x'-x)^2+(y'-y)^2+z^2}=tc/2$. Here, c is the speed of light and x,y,z are the spatial coordinates of the hidden volume. For convenience, we assume that the sampling locations x',y' are located on the plane $z=0$ and that the laser pulse is infinitesimally short, and we only consider indirect light transport that bounced precisely three times after emission by a light source and before being detected: off a visible surface within the line of sight, then off a hidden surface outside the line of sight, and finally, once more off the visible surface. The function g absorbs miscellaneous time-independent attenuation effects that depend on the hidden surface normals, reflectance properties of the hidden scene, visibility of a hidden point from some sampling point x',y' and several other factors. Each measurement in the confocal configuration integrates over spherical surfaces in the hidden scene. More general non-confocal configurations are also common, for which the detector samples the time-resolved indirect light transport at one point on the wall while the laser directly illuminates a different point on the visible surface[2,4]. The laser point or the detection point can then be scanned independently from each other. In this more general configuration, measurements integrate along elliptical surfaces. Moreover, higher-order bounces of indirect light transport could also be considered to model indirect reflections of light within the hidden scene, although these become increasingly difficult to measure.

This image formation model is at the core of most NLOS imaging approaches. The effects modelled by g make this a nonlinear image formation model. Several approaches work with a linearized approximation of Eq. 1, for which $g=1$. This linear approximation is easier to invert than the nonlinear model, but it makes several additional assumptions about the light transport in the hidden scene, such as that light scatters isotropically and no occlusions occur between different scene parts outside the line of sight. Indeed, line-of-sight imaging problems are made nonlinear in a similar fashion if surface normals, bidirectional reflectance distribution functions and occlusions are included in the model. This is why, typically, line-of-sight imaging systems also operate with linearized transport models. Various approaches to solving both the linearized and nonlinear NLOS problem are discussed below. The linearized problem reduces to approximating or solving the large linear equation system $\boldsymbol{\tau}=\boldsymbol{A}\boldsymbol{\rho}$, where $\boldsymbol{\tau}$ represents the discretized transient measurements, $\boldsymbol{\rho}$ are the unknown reflectance values of the hidden scene albedo, and $\boldsymbol{A}$ is a matrix describing the indirect time-resolved light transport.

Inverse methods

Heuristic solutions. Heuristic solutions for estimating the shape and reflectance of the hidden volume are popular. One of the most intuitive of these approaches is to relate the measured times of the first-returning indirect photons to the convex hull of the hidden object or scene[58]. Alternatively, simple parametric planar models can be fitted to represent the hidden scene[59]. Another area still in its infancy is the use of active capture methods, which shape illumination and detection to optimize capture based on the anticipated content of the scene. Spatial refocusing after the first scattering surface can be controlled using spatial light modulators, and the focused spot can be scanned across the scene[60]. Temporal focusing uses an illumination pulse that is shaped in space and time to create an illumination pulse at an area in the hidden scene[61]. These techniques can improve the signal-to-noise ratio and resolution for the obtained reconstruction.

Back-projection methods. Back-projection methods are some of the most popular methods for NLOS image reconstruction from transient measurements (FIG. 4a). They approximate the hidden volume (FIG. 4b) as $\boldsymbol{A}^{\mathrm{T}}\boldsymbol{\tau}$ and optionally apply a filtering or other post-processing step to this result (FIGS 2,4c). Similar strategies are standard practice for solving large-scale inverse problems, for example in medical imaging. Indeed, the inverse problem of confocal NLOS scanning approaches is closely related to the spherical Radon transform[62], whereas the general non-confocal scanning approach is similar to the elliptical Radon transform[63]. Filtered back-projection methods are standard solutions to these inverse problems. Both computational time and memory requirements of these Radon transforms are tractable even for large-scale inverse problems. Hence, several variants of back-projection algorithms have been explored for NLOS imaging[2,64–67], but when applied to NLOS imaging these algorithms have a computational complexity of $O(N^5)$ for N voxels. Like limited-baseline

tomography problems[68], NLOS problems are typically ill-posed inverse problems because acquired measurements usually do not sample all Fourier coefficients. In microscopy and medical imaging, this is known as the 'missing cone' problem. To estimate these missing components, the inverse method must incorporate statistical priors to fill in these parts using iterative solvers.

Linear inverse methods. Linear inverse methods have been proposed to solve the convex optimization problem of estimating $\boldsymbol{\rho}$ from $\boldsymbol{\tau}$. Several of these approaches aim to use iterative optimization methods to solve this problem[64,69,70], but such approaches are typically very slow. The light-cone transform (FIG. 4d) was proposed as a closed-form solution to the linear inverse problem, and it efficiently solves the exact linear inverse problem with a computational complexity of $O(N^3 \log N)$ by assuming a smoothness prior on the reconstructed volume[3]. An implementation of this method on graphics processing units has achieved real-time reconstruction rates[71].

Inverse light transport with partial occlusions, surfaces and normals. This class of methods has received much attention in recent research proposals, because some of the simplifying assumptions of the image formation model (Eq. 1) can be lifted by solving the nonlinear problem rather than a linearized approximation. For example, several time-resolved methods have included partial occlusions within the hidden scene in the image formation model[72–74]. Interestingly, it has been shown that occlusions and shadows in the hidden scene can also be exploited to facilitate passive NLOS approaches that do not require time-resolved imaging systems[9,10,75,76]. However, the associated inverse problems are much more ill-posed than they are for active imaging, and the proposed algorithms often make restrictive assumptions. A few recent approaches have also incorporated hidden surface normals into the image formation model[72,77], which can further help improve reconstruction quality. Finally, an emerging research direction is to reconstruct hidden surfaces, rather than volumes, directly from the transient measurements[77–80]. High-resolution volumes are memory-inefficient data structures and can quickly exceed available computational resources. Therefore, in practice, a trade-off between level of detail of a reconstructed volume and memory requirement may have to be made. Surface representations have the potential to represent finer geometric detail with fewer computational resources. It remains unclear, however, what the 'best' representation for general NLOS imaging is.

Wave optics models. These models — as opposed to the geometric optics model outlined above — have recently been explored for transient imaging configurations with time-resolved detectors and pulsed light sources[4,5,81–84] (FIGS 4,5). In these methods, the light transport in the hidden scene is modelled using the time-dependent wave equation or other models from physical optics. A similar concept was also applied to NLOS data captured in the Fourier domain by an amplitude-modulated continuous-wave light source[21].

The algorithms in this category do not necessarily try to solve the inverse problem of estimating the hidden geometry directly, unlike most of the methods discussed above. Rather, the transient image is treated as a virtual wave field and propagated backwards in time to a specific time instant. The geometry estimation problem then becomes that of relating the hidden geometry to specific properties of the temporally evolving wave field. As in a line-of-sight camera, the problem is thus divided into a linear operator that estimates the wave in the hidden scene (that is, the image) and a nonlinear problem of estimating properties such as geometry and bidirectional reflectance distribution functions from the image.

There are several benefits of a wave optics model for the NLOS problem. First, some of these approaches have been experimentally shown to be more robust to different types of reflectance properties of the hidden surfaces. Glossy, specular, diffuse or retro-reflective materials can all be treated with the same method, whereas geometric optics approaches must either know and model the reflectance properties a priori or estimate them along with the hidden geometry. Second, wave models make it easier to draw the connection between NLOS imaging and related work in areas such as radar, seismic imaging, ultrasonic imaging and other established fields. For example, range migration techniques, including frequency–wavenumber or *f*–*k* migration, originally developed in the seismic imaging community[85,86], and later adopted to synthetic aperture sonar[87,88], ultrasound imaging[89] and synthetic aperture radar[90], result in some of the fastest and most robust NLOS imaging techniques[5]. The phase information of the light wave used in these experiments is not measured or required. What is used instead is the phase and wavefront of an intensity wave riding on the optical carrier wave. The phase of this wave is related to the time of arrival of the signal photons, not to their optical phase. The phase of the light wave is typically not

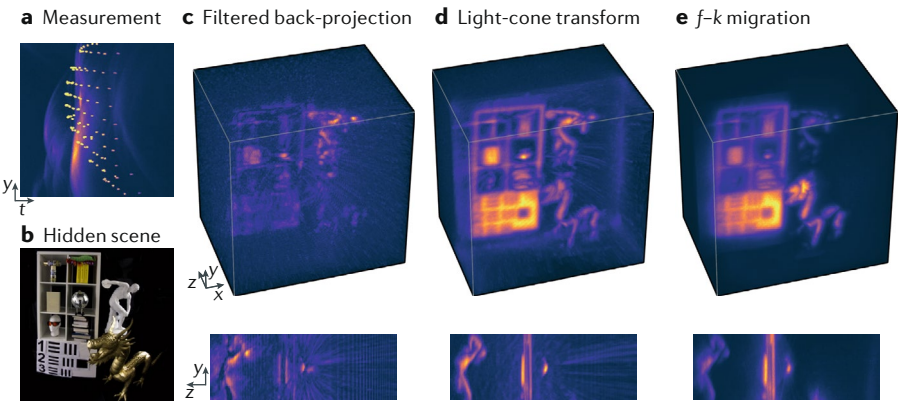

Fig. 4 | **NLOS reconstructions of a hidden room-sized scene. a,b** | One approach to non-line-of-sight (NLOS) imaging is to capture time-resolved measurements sampled across a visible surface and reconstruct the 3D shape and reflectance of the hidden scene. A disco ball produces the bright dots seen in the measurements of indirect light transport (panel **a**), and other diffuse and glossy objects produce the streaks. **c** | Of the methods for reconstructing shape and reflectance from these measurements, filtered back-projection is conceptually one of the simpler methods; it involves a delay-and-sum (that is, back-projection) operation of the time-resolved measurements, followed by a heuristic high-pass filter on the result. **d** | The light-cone transform is a fast reconstruction algorithm that produces more accurate reconstructions in less time than other approaches, but it requires the hidden objects to be either diffuse or highly reflective. **e** | NLOS imaging with frequency–wavenumber (*f*–*k*) migration is both fast and versatile. The wave-based nature of this inverse method is unique in being robust to objects with diverse and complex reflectance properties, such as the glossy dragon, the diffuse statue and the reflective disco ball shown in this scene. All volumes are rendered as maximum-intensity projections. Adapted with permission from REF.[5], Association for Computing Machinery.

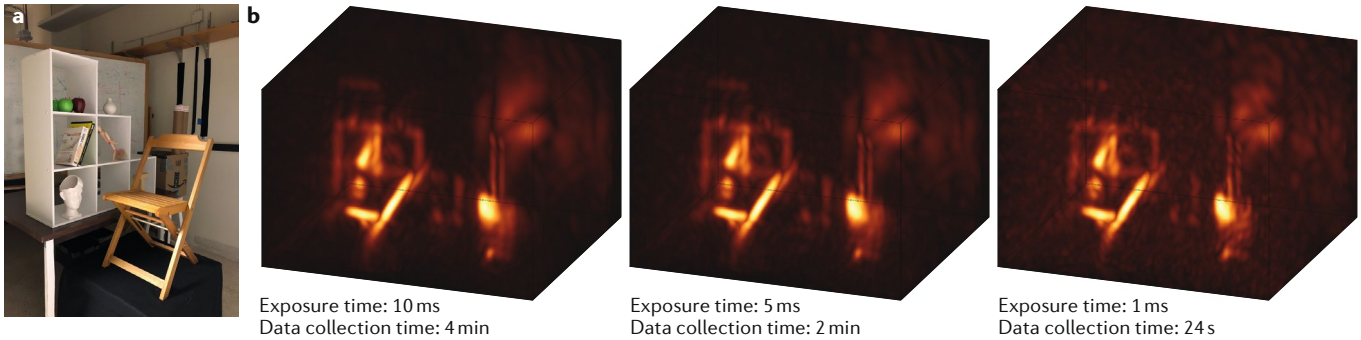

Fig. 5 | **Reconstructions of a large scene using the phasor-field virtual wave approach.** Data are collected with a single-pixel single-photon avalanche diode (SPAD), using point scanning to emulate a large detector array. **a** | The hidden scene. **b** | Reconstructions. The exposure time per scanned point and total data collection time is shown under each image in panel **b**. The entire scan involves 24,000 points. The scene is approximately 2 m wide and 3 m deep. Adapted from REF.[4], Springer Nature Limited.

accessible with time-resolved NLOS imaging systems. The time-of-flight information of indirect light transport must instead be used to estimate object shape, which makes the associated inverse problems different.

Data-driven approaches. Data-driven approaches are emerging as a tool for NLOS reconstructions. Neural networks can reconstruct hidden scenes from steady-state data captured with a continuous light source and a conventional camera[91,92]. However, practical application of neural networks to time-of-flight data faces the difficulty of generating sufficient training data. One approach could be to generate data numerically based on a known forward model. Recently, training data were experimentally collected using actual people, and these subsequently allowed NLOS classification of a small set of individuals and of their positions[93].

NLOS tracking. NLOS tracking of objects and people with time-resolved imaging systems is also an active area of research[3,52,55,94,95]. The tracking problem is substantially simpler than reconstructing a full hidden 3D volume, which makes it computationally more efficient to implement. These NLOS tracking approaches pave the way for future research that goes beyond hidden shape reconstruction and that could aim at classification[93], object detection, target identification or other inverse problems that build on transient light transport.

NLOS imaging without a relay wall. Most existing NLOS approaches require the imaging system to scan a large area on a visible surface, on which the indirect light paths of hidden objects are sampled. In many applications, however, optical access to a large scanning area may not be available. Inverse methods have been derived that exploit scene motion to simultaneously estimate both the shape and trajectory of a hidden object from transient images[96]. This problem is far more challenging and ill-posed than conventional NLOS imaging because the light transport is only measured along a single optical path, but it may further extend the application space of NLOS imaging techniques.

Resolution limits

The resolving power of conventional, diffraction-limited imaging systems is fundamentally limited by the numerical aperture of the optics and the wavelength at which they operate[97]. Time-resolved NLOS imaging also obeys fundamental resolution limits. These are primarily defined by two factors, namely the area on the visible surface over which the time-resolved indirect light transport of the hidden scene is recorded and the temporal resolution of the imaging system. The first factor, the scanning area, is analogous to the numerical aperture of a conventional imaging system — the larger the scanning area or numerical aperture, the better the transverse resolution. The second factor, temporal resolution, is somewhat analogous to the wavelength-limiting resolution of conventional systems. Together, these two characteristics of an NLOS imaging system define both transverse and axial resolution of a hidden volume, which can be estimated unambiguously — that is, without the use of statistical priors.

Formally, the resolution of an NLOS system is defined as the minimum resolvable distance of two scatterers. These two scattering points are resolvable in a hidden 3D space only if the measurements of their indirect reflections are resolvable in time. Assuming that the temporal resolution of the system is given by the full-width at half-maximum (FWHM) of its temporal impulse response, transverse and axial resolutions are

$$\Delta x \geq \frac{c \times \sqrt{w^2 + z^2}}{2w}\text{FWHM}, \qquad \Delta z \geq \frac{c \times \text{FWHM}}{2}. \tag{2}$$

Here, Δx and Δz are the minimum resolvable distance between the two scatterers in the transverse and axial dimension, respectively; c is the speed of light; z is the distance of the point scatterers from the visible surface; and the scanning area has a size of $2w \times 2w$. These resolution limits were derived for the confocal scanning configuration[3]. For non-confocal scanning configurations, the transverse resolution theoretically decreases by a factor of 2. Other works have also used signal processing techniques[98], linear systems approaches[99] or feature visibility[100] to bound localization and photometric error in NLOS imaging scenarios.

Other NLOS imaging approaches

It is worth mentioning that there are other techniques that do not require transient light imaging capability.

Steady-state systems use a continuous spatially confined light source and a slow conventional camera or detector to detect spatial variations in the return light. In these systems, integration times of the detector are long enough to consider the time of flight of the light to be infinite, and what is detected is always a steady-state scene response. For example, the location of a single hidden object can be estimated when using a shortwave infrared light source and camera[101]. An intriguing modification of the

steady-state approach is to use occlusions in the scene, such as edges, to provide additional spatial information, and to rely on motion and differential measurements to eliminate problems with background light. In suitable scenes, these methods can provide detailed information about objects in the scene using inexpensive, passive visible light cameras and natural ambient light sources[9–11,73,76,92,102]. In interferometric approaches, the scene is illuminated with a coherent light source, and interference patterns in the returned light are analysed. For example, the spatial speckle of the returned light can be collected and analysed to reconstruct 2D NLOS images[7]. This method makes use of the memory effect that preserves angular information in the interaction with thin scatterers. Doing so limits existing demonstrations to imaging very small objects, covering a solid angle of no more than several degrees when viewed from the wall. This limitation could probably be improved by incorporating more information, such as speckle patterns from multiple coherent light sources. Spatial correlations within the reflected light from an observation wall can also be used to directly retrieve information of a hidden scene, made up of active yet incoherent light sources[103], for example. Extending this concept to the temporal domain (that is, tracking the temporal correlations within the reflected beam) enables a time-of-flight approach with an impressive 10-fs resolution[11]. We have also already mentioned adaptive shaping of the illuminating laser beam that can transform the wall into a mirror by using an input spatial phase on the beam that compensates for scattering from the first surface. This makes it possible to scan a focused spot across the scene and retrieve image information from the reflected light intensity during the scan[60]. Finally, deep learning techniques have recently been demonstrated to provide a useful framework to solve challenging inverse correlography problems arising in interferometric NLOS approaches[104].

Another group of interferometric methods is based on illuminating the hidden scene with a pulsed coherent source via the relay surface and interfering the returning light with a delayed local oscillator light beam derived from the same coherent illumination source. This process can be thought of as a coherent time gating method that produces data that can be treated similarly to data from other time-resolved detectors. An example of this used a set-up similar to a time-domain optical coherence tomography system[20]. Interference is used in this case as a coherence gate to determine the time of flight of the light through the scene. The need for an adjustable optical delay line complicates this set-up. Another approach uses interference between the speckle patterns created by a NLOS object; the reconstruction is obtained by combining the results from different illumination frequencies. This procedure has the same effect as using a short pulse but eliminates the need for a delay line. Other efforts into coherent NLOS imaging include speckle interferometry to detect motion[105,106].

Table 1 | **Methods and requirements for the most common reconstruction techniques**

Reconstruction method	Light source	Detector	Refs
Detection or localization	High-repetition/single-shot laser	SPAD or APD	55,107
Backpropagation	High-repetition laser	Streak camera, SPAD array	2,56
Light-cone transform, *f*–*k* migration	High-repetition laser	SPAD array	3,5
Virtual/phasor field	High-repetition laser	SPAD or SPAD array	4,82–84
Steady-state, occlusions, coherence	CW laser, ambient light	Standard CMOS camera, APD	7,10,101,102
Machine learning	Pulsed or continuous-wave laser	SPADs, standard CMOS camera	91–93,104

More details and references are provided in the main text. APD, avalanche photodiode; CMOS, complementary metal–oxide–semiconductor; *f*–*k*, frequency–wavenumber; SPAD, single-photon avalanche diode.

Conclusions and future directions

LiDAR systems are emerging as a standard imaging modality in autonomous driving, robotics, remote sensing and defence. The same detectors — avalanche photodiodes (APDs) and SPADs — are also increasingly used in consumer electronics, fluorescence lifetime microscopy and positron emission tomography. SPADs in particular are an ideal platform for extending LiDAR to NLOS imaging because they address two primary challenges: being able to detect a few, indirectly reflected photons among many, and time-stamping the photon time of arrival with high accuracy.

The ability to image objects outside the direct line of sight is likely to be most useful for applications that already use LiDAR systems. For instance, self-driving cars could sense obstacles beyond the next bend or in front of the car ahead, and could more safely navigate around them. Eventually, NLOS imaging could become a software upgrade in existing or future LiDAR systems. For this reason, we believe that such time-resolved NLOS imaging systems are one of the most promising directions in this emerging research area.

There are multiple approaches and options for NLOS imaging, even when restricted to time-of-flight techniques. The main techniques discussed here are summarized in TABLE 1 and FIG. 6, together with their hardware requirements (based on present-day implementations). Each approach has its own advantages, and these need to be weighed when considering a particular application. For example, some NLOS LiDAR applications for the automotive industry may not require full 3D reconstruction of a scene but instead will benefit from a much simpler approach geared towards locating the position of a hidden object and identifying its nature (such as human, car or bicycle). Compared with alternative methods to image occluded spaces, such as transmitted or reflected radar, X-ray transmission, reflected acoustic imaging or the placement of mobile cameras or mirrors, optical NLOS imaging has the potential to work in real time, particularly for large detector-to-scene (that is, 'stand-off') distances, albeit with targets that are limited to distances of 2–3 m behind the obstacle. This kind of task becomes even more favourable when the hidden object is in movement, in which case subtraction of the background is straightforward and has already been demonstrated to work at stand-off distances of 50 m or more in daylight. Recent reports indicate stand-off distances of 1.4 km. Simple range-finding from behind an obstacle can also be achieved with a single-shot measurement if APDs rather than SPADs are used, as APDs can collect multiple photons from a single, high-energy return signal[107].

However, there are scenarios in which full 3D imaging is indeed desired, for example in reconnaissance missions or in situations for which 3D information of an otherwise inaccessible area is needed. Examples that we have encountered range from identification of suitable underground cave sites for future manned planet missions to decommissioning

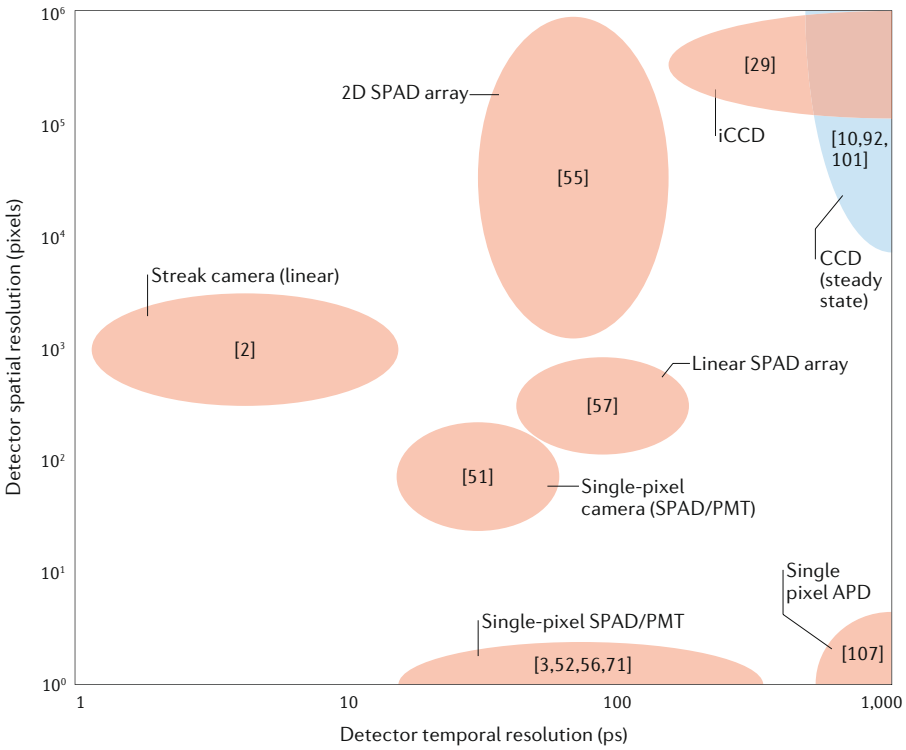

Fig. 6 | **Main detector technologies classified based on spatial and temporal resolution.** Steady-state detector technologies (that is, using non-time-resolving detectors such as charge-coupled device (CCD) or complementary metal–oxide–semiconductor (CMOS) cameras) are shown in blue, to differentiate these from time-of-flight technologies. Some detector formats are linear (1D), as indicated in the figure. References in square brackets indicate example uses of each technology. APD, avalanche photodiode; iCCD, intensified CCD; PMT, photomultiplier tube; SPAD, single-photon avalanche diode.

of radioactive nuclear fission test facilities. In these situations, the longer acquisition times required for 3D reconstruction and high laser powers may be less of an issue and an acceptable compromise. Existing systems could potentially already successfully tackle such tasks.

Finally, there is scope for future work combining the optical NLOS imaging techniques outlined in this Perspective with other technologies. For example, radar and WiFi can provide partial information directly through certain kinds of wall[108–113]. Approaches based on sound[8] have also been proposed. These and other technologies could potentially complement each other, either through direct data fusion that increases the collected information, or by using one approach to provide coarse-grained information that would indicate the interest or need to continue with fine-grained optical techniques.

Daniele Faccio[1✉], *Andreas Velten*[2,3] *and Gordon Wetzstein*[4]

[1]*School of Physics and Astronomy, University of Glasgow, Glasgow, UK.*

[2]*Department of Biostatistics and Medical Informatics, University of Wisconsin–Madison, Madison, WI, USA.*

[3]*Department of Electrical and Computer Engineering, University of Wisconsin–Madison, Madison, WI, USA.*

[4]*Department of Electrical Engineering, Stanford University, Stanford, CA, USA.*

✉*e-mail: daniele.faccio@glasgow.ac.uk*

https://doi.org/10.1038/s42254-020-0174-8
Published online: 13 May 2020

1. Kirmani, A., Hutchison, T., Davis, J. & Raskar, R. Looking around the corner using transient imaging. *Proc. IEEE Int. Conf. Comput. Vis.* **2009**, 159–166 (2009).
2. Velten, A. et al. Recovering three-dimensional shape around a corner using ultrafast time-of-flight imaging. *Nat. Commun.* **3**, 745 (2012).
Report of full 3D NLOS imaging.
3. O'Toole, M., Lindell, D. B. & Wetzstein, G. Confocal non-line-of-sight imaging based on the light-cone transform. *Nature* **555**, 338 (2018).
Report applying light-cone transform and producing high-quality 3D reconstructions over a large NLOS area.
4. Liu, X. et al. Non-line-of-sight imaging using phasor-field virtual wave optics. *Nature* **572**, 620–623 (2019).
Virtual-wave reconstruction approach for fast and detailed NLOS scene reconstruction.
5. Lindell, D. B., Wetzstein, G. & O'Toole, M. Wave-based non-line-of-sight imaging using fast *f*–*k* migration. *ACM Trans. Graph.* **38**, 116 (2019).
A fast and accurate wave-optics method for 3D NLOS imaging at interactive frame-rates.
6. Bertolotti, J. et al. Non-invasive imaging through opaque scattering layers. *Nature* **491**, 232–234 (2012).
7. Katz, O., Heidmann, P., Fink, M. & Gigan, S. Non-invasive single-shot imaging through scattering layers and around corners via speckle correlations. *Nat. Photonics* **8**, 784–790 (2014).
Correlation technique for diffuse and NLOS imaging that does not rely on time-of-flight measurements.
8. Lindell, D. B., Wetzstein, G. & Koltun, V. Acoustic non-line-of-sight imaging. *Proc. IEEE Conf. Comput. Vis. Pattern Recognit.* **2019**, 6773–6782 (2019).
9. Bouman, K. L. et al. Turning corners into cameras: principles and methods. *Proc. IEEE Int. Conf. Comput. Vis.* **2017**, 2289–2297 (2017).
10. Saunders, C., Murray-Bruce, J. & Goyal, V. K. Computational periscopy with an ordinary digital camera. *Nature* **565**, 472–475 (2019).
A passive NLOS approach that relies on lighting in the scene and uses ordinary cameras.
11. Boger-Lombard, J. & Katz, O. Non line-of-sight localization by passive optical time-of-flight. *Nat. Commun.* **10**, 3343 (2019).
12. Maeda, T., Wang, Y., Raskar, R. & Kadambi, A. Thermal non-line-of-sight imaging. *Proc. IEEE Int. Conf. Comput. Photogr.* **2019**, 1–11 (2019).
13. Kaga, M. et al. Thermal non-line-of-sight imaging from specular and diffuse reflections. *IPSJ Trans. Comp. Vis. Appl.* **11**, 8 (2019).
14. Faccio, D. & Velten, A. A trillion frames per second: the techniques and applications of light-in-flight photography. *Rep. Prog. Phys.* **81**, 105901 (2018).
Review paper on transient imaging.
15. Hariharan, P. *Basics of Holography* (Cambridge Univ. Press, 2011).
16. Abramson, N. Light-in-flight recording by holography. *Opt. Lett.* **3**, 121 (1978).
17. Abramson, N. Light-in-flight recording: high-speed holographic motion pictures of ultrafast phenomena. *Appl. Opt.* **22**, 215–232 (1983).
18. Abramson, N. Light-in-flight recording. 4: Visualizing optical relativistic phenomena. *Appl. Opt.* **24**, 3323–3329 (1985).
19. Abramson, N. *Light in Flight or the Holodiagram: The Columbi Egg of Optics* (SPIE, 1998).
20. Gkioulekas, I., Levin, A., Durand, F. & Zickler, T. Micron-scale light transport decomposition using interferometry. *ACM Trans. Graph.* **34**, 37 (2015).
21. Kadambi, A. et al. Coded time of flight cameras: sparse deconvolution to address multipath interference and recover time profiles. *ACM Trans. Graph.* **32**, 1–167 (2013).
22. Heide, F., Hullin, M. B., Gregson, J. & Heidrich, W. Low-budget transient imaging using photonic mixer devices. *ACM Trans. Graph.* **32**, 45:1–45:10 (2013).
23. Peters, C., Klein, J., Hullin, M. B. & Klein, R. Solving trigonometric moment problems for fast transient imaging. *ACM Trans. Graph.* **34**, 220 (2015).
24. Jarabo, A., Masia, B., Marco, J. & Gutierrez, D. Recent advances in transient imaging: a computer graphics and vision perspective. *Vis. Inform.* **1**, 65–79 (2017).
25. Velten, A. et al. Femto-photography: capturing and visualizing the propagation of light. *ACM Trans. Graph.* **32**, 44:1–44:8 (2013).
26. Gao, L., Liang, J., Li, C. & Wang, L. V. Single-shot compressed ultrafast photography at one hundred billion frames per second. *Nature* **516**, 74–77 (2014).
27. Mikami, H., Gao, L. & Goda, K. Ultrafast optical imaging technology: principles and applications of emerging methods. *Nanophotonics* **5**, 98–110 (2016).
28. Zhu, L. et al. Space- and intensity-constrained reconstruction for compressed ultrafast photography. *Optica* **3**, 694–697 (2016).
29. Laurenzis, M. & Velten, A. Nonline-of-sight laser gated viewing of scattered photons. *Opt. Eng.* **53**, 53–53–7 (2014).
30. Jarabo, A. et al. Relativistic effects for time-resolved light transport. *Comput. Graph. Forum* **34**, 1–12 (2015).
31. Laurenzis, M., Klein, J. & Bacher, E. Relativistic effects in imaging of light in flight with arbitrary paths. *Opt. Lett.* **41**, 2001–2004 (2016).
32. Clerici, M. et al. Observation of image pair creation and annihilation from superluminal scattering sources. *Sci. Adv.* **2**, e1501691 (2016).
33. Strutt, J. W. (Baron Rayleigh). *Theory of Sound* (MacMillan, 1896).
34. Becker, W. *Advanced Time-Correlated Single Photon Counting Techniques* (Springer, 2005).
35. Niclass, C., Gersbach, M., Henderson, R., Grant, L. & Charbon, E. A single photon avalanche diode implemented in 130-nm CMOS technology. *IEEE J. Sel. Top. Quantum Electron.* **13**, 863–869 (2007).

36. Richardson, J. et al. A 32×32 50 ps resolution 10 bit time to digital converter array in 130 nm CMOS for time correlated imaging. *Proc. IEEE Custom Integr. Circuits Conf.* **2009**, 77–80 (2009).
37. Richardson, J. A., Webster, E. A. G., Grant, L. A. & Henderson, R. K. Scaleable single-photon avalanche diode structures in nanometer CMOS technology. *IEEE Trans. Electron. Devices* **58**, 2028–2035 (2011).
38. Gersbach, M. et al. A time-resolved, low-noise single-photon image sensor fabricated in deep-submicron CMOS technology. *IEEE J. Solid-State Circuits* **47**, 1394–1407 (2012).
39. Bronzi, D. et al. 100 000 frames/s 64×32 single-photon detector array for 2-D imaging and 3-D ranging. *IEEE J. Sel. Top. Quantum Electron.* **20**, 354–363 (2014).
40. Kramer, B. et al. A SPAD array detector for spectrally and lifetime resolved microscopy (Poster). *17th Int. Workshop Single Mol. Spectrosc. Ultrasensitive Anal. Life Sci.* **69** (2011).
41. Cammi, C., Gulinatti, A., Rech, I., Panzeri, F. & Ghioni, M. Spad array module for multi-dimensional photon timing applications. *J. Mod. Opt.* **59**, 131–139 (2012).
42. Zappa, F. & Tosi, A. MiSPIA: microelectronic single-photon 3D imaging arrays for low-light high-speed safety and security applications. *Proc. SPIE* **8727**, 87270L (2013).
43. Veerappan, C. et al. A 160×28 single-photon image sensor with on-pixel 55 ps 10 bit time-to-digital converter. *Proc. IEEE Int. Solid-State Circuits Conf.* **2011**, 312–314 (2011).
44. Villa, F., Lussana, R., Tamborini, D., Tosi, A. & Zappa, F. High-fill-factor 60×1 SPAD array with 60 subnanosecond integrated TDCs. *IEEE Photonics Technol. Lett.* **27**, 1261–1264 (2015).
45. Burri, S., Homulle, H., Bruschini, C. & Charbon, E. LinoSPAD: a time-resolved 256×1 CMOS SPAD line sensor system featuring 64 FPGA-based TDC channels running at up to 8.5 giga-events per second. *Proc. SPIE* **9899**, 98990D (2016).
46. Abbas, T. A. et al. Backside illuminated SPAD image sensor with 7.83 μm pitch in 3D-stacked CMOS technology. *Proc. IEEE Int. Electron Devices Meet.* **2016**, 8.1.1–8.1.4 (2016).
47. Itzler, M., Jiang, X., Ben-Michael, R., Nyman, B. & Slomkowski, K. Geiger-mode APD single photon detectors. *Proc. Opt. Fiber Commun. Conf.* **2008**, 1–3 (2008).
48. Itzler, M., Jiang, X., Ben-Michael, R., Nyman, B. & Slomkowski, K. Single photon avalanche photodiodes for near-infrared photon counting. *SPIE Proc.* **6900**, 69001E (2008).
49. Itzler, M. A. et al. Single photon avalanche diodes (SPADs) for 1.5 μm photon counting applications. *J. Mod. Opt.* **54**, 283–304 (2007).
50. Gariepy, G. et al. Single-photon sensitive light-in-flight imaging. *Nat. Commun.* **6**, 6021 (2015).
51. Musarra, G. et al. Non-line-of-sight 3D imaging with a single-pixel camera. *Phys. Rev. Appl.* **12**, 011002 (2019).
52. Chan, S., Warburton, R., Gariepy, G., Leach, J. & Faccio, D. Non-line-of-sight tracking of people at long range. *Opt. Express* **25**, 10109 (2017).
53. Lindell, D. B., O'Toole, M. & Wetzstein, G. Towards transient imaging at interactive rates with single-photon detectors. *Proc. IEEE Int. Conf. Comput. Photogr.* **2018**, 1–8 (2018).
54. Pawlikowska, A. M., Halimi, A., Lamb, R. A. & Buller, G. S. Single-photon three-dimensional imaging at up to 10 kilometers range. *Opt. Express* **25**, 11919 (2017).
55. Gariepy, G., Tonolini, F., Henderson, R., Leach, J. & Faccio, D. Detection and tracking of moving objects hidden from view. *Nat. Photonics* **10**, 23–26 (2016).
Real-time tracking of a moving NLOS object.
56. Buttafava, M., Zeman, J., Tosi, A., Eliceiri, K. & Velten, A. Non-line-of-sight imaging using a time-gated single photon avalanche diode. *Opt. Express* **23**, 20997–21011 (2015).
57. O'Toole, M. et al. Reconstructing transient images from single-photon sensors. *Proc. IEEE Conf. Comput. Vis. Pattern Recognit.* **2017**, 2289–2297 (2017).
58. Tsai, C.-Y., Kutulakos, K. N., Narasimhan, S. G. & Sankaranarayanan, A. C. The geometry of first-returning photons for non-line-of-sight imaging. *Proc. IEEE Conf. Comput. Vis. Pattern Recognit.* **2017**, 7216–7224 (2017).
59. Pediredla, A. K., Buttafava, M., Tosi, A., Cossairt, O. & Veeraraghavan, A. Reconstructing rooms using photon echoes: a plane based model and reconstruction algorithm for looking around the corner. *Proc. IEEE Int. Conf. Comput. Photogr.* **2017**, 1–12 (2017).
60. Starshynov, I., Ghafur, O., Fitches, J. & Faccio, D. Coherent control of light for non-line-of-sight imaging. Preprint at *arXiv* https://arxiv.org/abs/1908.04094 (2019).
61. Pediredla, A., Dave, A. & Veeraraghavan, A. Snlos: Non-line-of-sight scanning through temporal focusing. *Proc. EEE Int. Conf. Comput. Photogr.* **2019**, 1–13 (2019).
62. Tasinkevych, J. & Trots, I. Circular radon transform inversion technique in synthetic aperture ultrasound imaging: an ultrasound phantom evaluation. *Arch. Acoust.* **39**, 569–582 (2014).
63. Moon, S. On the determination of a function from an elliptical radon transform. *J. Math. Anal. Appl.* **416**, 724–734 (2014).
64. Gupta, O., Willwacher, T., Velten, A., Veeraraghavan, A. & Raskar, R. Reconstruction of hidden 3D shapes using diffuse reflections. *Opt. Express* **20**, 19096–19108 (2012).
65. Buttafava, M., Boso, G., Ruggeri, A., Mora, A. D. & Tosi, A. Time-gated single-photon detection module with 110 ps transition time and up to 80 MHz repetition rate. *Rev. Sci. Instrum.* **85**, 083114 (2014).
66. Laurenzis, M. & Velten, A. Feature selection and back-projection algorithms for nonline-of-sight laser-gated viewing. *J. Electron. Imaging* **23**, 063003 (2014).
67. Arellano, V., Gutierrez, D. & Jarabo, A. Fast back-projection for non-line of sight reconstruction. *Opt. Express* **25**, 11574–11583 (2017).
68. Kak, A. C., Slaney, M. & Wang, G. Principles of computerized tomographic imaging. *Med. Phys.* **29**, 107–107 (2002).
69. Wu, D. et al. Frequency analysis of transient light transport with applications in bare sensor imaging. *Proc. 12th Eur. Conf. Comput. Vis.* **7572**, 542–555 (2012).
70. Heide, F., Xiao, L., Heidrich, W. & Hullin, M. B. Diffuse mirrors: 3D reconstruction from diffuse indirect illumination using inexpensive time-of-flight sensors. *Proc. IEEE Conf. Comput. Vis. Pattern Recognit.* **2014**, 3222–3229 (2014).
A low-cost approach to NLOS imaging over short distances.
71. O'Toole, M., Lindell, D. B. & Wetzstein, G. Real-time non-line-of-sight imaging. In *ACM SIGGRAPH Emerging Technologies* 14 (ACM, 2018).
72. Heide, F. et al. Non-line-of-sight imaging with partial occluders and surface normals. *ACM Trans. Graph.* **38**, 22 (2019).
73. Thrampoulidis, C. et al. Exploiting occlusion in non-line-of-sight active imaging. *IEEE Trans. Computational Imaging* **4**, 419–431 (2018).
74. Xu, F. et al. Revealing hidden scenes by photon-efficient occlusion-based opportunistic active imaging. *Opt. Express* **26**, 9945–9962 (2018).
75. Seidel, S. W. et al. Corner occluder computational periscopy: estimating a hidden scene from a single photograph. *Proc. IEEE Int. Conf. Comput. Photogr.* **2019**, 1–9 (2019).
76. Baradad, M. et al. Inferring light fields from shadows. *Proc. IEEE Conf. Comput. Vis. Pattern Recognit.* **2018**, 6267–6275 (2018).
77. Xin, S. et al. A theory of Fermat paths for non-line-of-sight shape reconstruction. *Proc. IEEE Conf. Comput. Vis. Pattern Recognit.* **2019**, 6800–6809 (IEEE, 2019).
78. Iseringhausen, J. & Hullin, M. B. Non-line-of-sight reconstruction using efficient transient rendering. Preprint at *arXiv* https://arxiv.org/abs/1809.08044 (2018).
79. Tsai, C.-Y., Sankaranarayanan, A. C. & Gkioulekas, I. Beyond volumetric albedo — a surface optimization framework for non-line-of-sight imaging. *Proc. IEEE Conf. Comput. Vis. Pattern Recognit.* **2019**, 1545–1555 (2019).
80. Young, S., Lindell, D. & Wetzstein, G. Non-line-of-sight surface reconstruction using the directional light-cone transform. In *IEEE Conf. Comput. Vis. Pattern Recognit.* (IEEE, 2020).
81. Reza, S. A., La Manna, M. & Velten, A. A physical light transport model for non-line-of-sight imaging applications. Preprint at *arXiv* https://arxiv.org/abs/1802.01823 (2018).
82. Teichman, J. A. Phasor field waves: a mathematical treatment. *Opt. Express* **27**, 27500–27506 (2019).
83. Reza, S. A., Manna, M. L., Bauer, S. & Velten, A. Phasor field waves: experimental demonstrations of wave-like properties. *Opt. Express* **27**, 32587–32608 (2019).
84. Dove, J. & Shapiro, J. H. Paraxial theory of phasor-field imaging. *Opt. Express* **27**, 18016–18037 (2019).
85. Stolt, R. H. Migration by Fourier transform. *Geophysics* **43**, 23–48 (1978).
86. Margrave, G. F. & Lamoureux, M. P. *Numerical Methods of Exploration Seismology: with Algorithms in MATLAB* (Cambridge Univ. Press, 2018).
87. Callow, H. J. *Signal Processing for Synthetic Aperture Sonar Image Enhancement.* Thesis, Univ. Canterbury (2003).
88. Sheriff, R. W. Synthetic aperture beamforming with automatic phase compensation for high frequency sonars. *Proc. IEEE Symp. Auton. Underwater Veh. Technol.* **1992**, 236–245 (1992).
89. Garcia, D. et al. Stolt's *fk* migration for plane wave ultrasound imaging. *IEEE Trans. Ultrason. Ferroelectr. Freq. Control.* **60**, 1853–1867 (2013).
90. Cafforio, C., Prati, C. & Rocca, F. SAR data focusing using seismic migration techniques. *IEEE Trans. Aerosp. Electron. Syst.* **27**, 194–207 (1991).
91. Tancik, M., Swedish, T., Satat, G. & Raskar, R. Data-driven non-line-of-sight imaging with a traditional camera. In *Imaging Appl. Opt.* (Optical Society of America, 2018).
92. Chen, W., Daneau, S., Mannan, F. & Heide, F. Steady-state non-line-of-sight imaging. *Proc. IEEE Conf. Comput. Vis. Pattern Recognit.* **2019**, 6790–6799 (2019).
93. Caramazza, P. et al. Neural network identification of people hidden from view with a single-pixel, single-photon detector. *Sci. Rep.* **8**, 11945 (2018).
94. Pandharkar, R. et al. Estimating motion and size of moving non-line-of-sight objects in cluttered environments. *Proc. IEEE Conf. Comput. Vis. Pattern Recognit.* **2011**, 265–272 (2011).
95. Chan, S., Warburton, R., Gariepy, G., Leach, J. & Faccio, D. Real-time tracking of hidden objects with single-pixel detectors. *Electron. Lett.* **53**, 1005–1008 (2017).
96. Metzler, C. A., Lindell, D. B. & Wetzstein, G. Keyhole imaging: Non-line-of-sight imaging and tracking of moving objects along a single optical path at long standoff distances. Preprint at *arXiv* https://arxiv.org/abs/1912.06727 (2019).
97. Born, M. & Wolf, E. *Principles of Optics: Electromagnetic Theory of Propagation, Interference and Diffraction of Light* (Elsevier, 2013).
98. Kadambi, A., Zhao, H., Shi, B. & Raskar, R. Occluded imaging with time-of-flight sensors. *ACM Trans. Graph.* **35**, 15 (2016).
99. Pediredla, A. K., Matsuda, N., Cossairt, O. & Veeraraghavan, A. Linear systems approach to identifying performance bounds in indirect imaging. *Proc. IEEE Int. Conf. Acoust. Speech Signal Process.* **2017**, 6235–6239 (2017).
100. Liu, X., Bauer, S. & Velten, A. Analysis of feature visibility in non-line-of-sight measurements. *Proc. IEEE Conf. Comput. Vis. Pattern Recognit.* **2019**, 10140–10148 (2019).
101. Klein, J., Peters, C., Martín, J., Laurenzis, M. & Hullin, M. B. Tracking objects outside the line of sight using 2D intensity images. *Sci. Rep.* **6**, 32491 (2016).
102. Torralba, A. & Freeman, W. T. Accidental pinhole and pinspeck cameras: revealing the scene outside the picture. *Proc. IEEE Conf. Comput. Vis. Pattern Recognit.* **2012**, 374–381 (2012).
103. Batarseh, M. et al. Passive sensing around the corner using spatial coherence. *Nat. Commun.* **9**, 3629 (2018).
104. Metzler, C. A. et al. Deep-inverse correlography: towards real-time high-resolution non-line-of-sight imaging. *Optica* **7**, 63–71 (2020).
105. Willomitzer, F., Li, F., Balaji, M. M., Rangarajan, P. & Cossairt, O. High resolution non-line-of-sight imaging with superheterodyne remote digital holography. In *Imaging Appl. Opt.* CM2A.2 (Optical Society of America, 2019).
106. Rangarajan, P., Willomitzer, F., Cossairt, O. & Christensen, M. P. Spatially resolved indirect imaging of objects beyond the line of sight. *Proc. SPIE* **11135**, 124–131 (2019).

107. Brooks, J. & Faccio, D. A single-shot non-line-of-sight range-finder. *Sensors* **19**, 4820 (2019).
108. Nkwari, P. K. M., Sinha, S. & Ferreira, H. C. Through-the-wall radar imaging: a review. *IETE Tech. Rev.* **35**, 631–639 (2018).
109. Amin, M. G. *Through-the-wall RADAR Imaging* (CRC, 2011).
110. Sume, A. et al. Radar detection of moving targets behind corners. *IEEE Trans. Geosci. Remote. Sens.* **49**, 2259–2267 (2011).
111. Nag, S., Barnes, M. A., Payment, T. & Holladay, G. Ultrawideband through-wall radar for detecting the motion of people in real time. *Proc. SPIE* **4744**, 48–57 (2002).
112. Ralston, T., Charvat, G. & Peabody, J. Real-time through-wall imaging using an ultrawideband multiple-input multiple-output (MIMO) phased array radar system. *IEEE Int. Symp. Phased Array Syst. Technol.* **2010**, 551–558 (2010).
113. Zhao, M. et al. Through-wall human pose estimation using radio signals. *Proc. IEEE Conf. Comput. Vis. Pattern Recognit.* **2018**, 7356–7365 (2018).

Acknowledgements
G.W. and A.V. acknowledge financial support from DARPA REVEAL (HR0011-16-C-0025). G.W. is supported by NSF CAREER Award (IIS 1553333), PECASE (ARO, W911NF19-1-0120) and the Visual Computing Center CCF grant (KAUST Office of Sponsored Research). D.F. is supported by the Royal Academy of Engineering under the Chairs in Emerging Technologies scheme and by the EPSRC (UK, grant no. EP/T00097X/1).

Author contributions
All authors contributed to all aspects of manuscript preparation, revision and editing.

Competing interests
The authors declare no competing interests.

Peer review information
Nature Reviews Physics thanks E. Charbon, K. Kutulakos and S. Gigan for their contribution to the peer review of this work.

Publisher's note
Springer Nature remains neutral with regard to jurisdictional claims in published maps and institutional affiliations.